Josephson-vortex-flow terahertz emission in layered high-T_c superconducting single crystals

Myung-Ho Bae[1], Hu-Jong Lee[1,2], and Jae-Hyun Choi[1]
[1] *Department of Physics, Pohang University of Science and Technology, Pohang 790-784, Republic of Korea and*
[2] *National Center for Nanomaterials Technology, Pohang 790-784, Republic of Korea*
(Dated: February 6, 2008)

We report on the successful terahertz emission (0.6∼1 THz) that is continuous and tunable in its frequency and power, by driving Josephson vortices in resonance with the collective standing Josephson plasma modes excited in stacked $Bi_2Sr_2CaCu_2O_{8+x}$ intrinsic Josephson junctions. Shapiro-step detection was employed to confirm the terahertz-wave emission. Our results provide a strong feasibility of developing long-sought solid-state terahertz-wave emission devices.

PACS numbers: 74.72.Hs, 74.50.+r, 74.78.Fk, 85.25.Cp

Rapidly increasing applications of the electromagnetic (EM) waves in the terahertz frequency range (∼0.1-30 THz) to nondestructive diagnosis, safe medical imaging, security measures and inspections, high-speed communications, etc., demand a novel technique of efficient terahertz-wave generation. Semiconductor EM-wave generating elements, covering a wide-range of frequency spectra, mainly rely on two operation principles: sinusoidal current oscillation and the transition of electronic states between quantum levels, which are realized by electronic and photonic means, respectively. However, terahertz-range EM-wave technology has remained underdeveloped due to the following reasons: (i) in electronics, the transit of charge carriers in a semiconductor device inherently takes too long to produce the terahertz oscillation, while (ii) in photonics, the terahertz-range photon energy is much lower than the room-temperature ambient thermal energy. This lack of generating technology in the terahertz band is often dubbed the "terahertz gap". In spite of recent progress in assorted generation techniques [1, 2, 3, 4] the terahertz generation remains to be a subject of intensive research efforts.

The present work describes the direct detection of the Josephson vortex-flow-induced terahertz-wave emission from $Bi_2Sr_2CaCu_2O_{8+x}$ (Bi-2212) stacked intrinsic Josephson junctions (IJJs). Since the size of the superconducting gap in Bi-2212 is higher than the Josephson plasma edge both the emission and the detection are allowed in a terahertz range [5]. In this study, the terahertz-wave emission was confirmed by observing Shapiro steps in an on-chip stack of IJJs (detector stack) as it was irradiated by the emission from the oscillator stack. The frequency of the emitted wave was tuned by the bias voltage, while the emission power was controlled by the bias current and switching of the resonating modes.

Naturally grown layered high-T_c superconducting Bi-2212 single crystals contain IJJs [6], where a 0.3-nm-thick superconducting CuO_2 bi-layer and a 1.2-nm-thick insulating BiO-SrO layer alternate along the c axis. Since the superconducting electrodes in IJJs are much thinner than the c-axis London penetration depth λ_{ab} (∼200 nm) the phase parameter ϕ_n in the nth Josephson junction is inductively coupled to those of neighboring junctions [7, 8]. Thus, the electrodynamics, governed by coupled Sine-Gordon differential equations in a system of N stacked IJJs, is represented by the same number of standing Josephson plasma (SJP) collective eigen modes formed along the c-axis direction. Josephson vortices generated by a planar external magnetic field tend to move in a tunneling bias current in resonance with the collective SJP modes, with the spatial phase distribution ranging from a rectangular (in-phase) to a triangular (out-of-phase) lattice. The Josephson-vortex-induced emission power can be enhanced by tuning the vortex lattice closer to the in-phase rectangular mode [9].

The conventional solid-state-reaction method was adopted to prepare Bi-2212 single crystals, which were slightly overdoped. The double-side-cleaving technique [10] was then employed to isolate and sandwich a finite number of Bi-2212 IJJs between two Au electrodes, essentially eliminating the interference from the pedestals (stacks of IJJs outside of but coupled to the stack of IJJs of interest) and thus allowing the formation of ideal multiple SJP modes along the c-axis direction. We fabricated two specimens of stacked IJJs (SP1 and SP2) sandwiched between two Au electrodes. Detailed fabrication procedures are described in Ref. [11]. Figs. 1(a) and (b) show the schematic of the typical sample configuration and an SEM image of SP2, respectively. The oscillator stacks were 13.5×1.4 μm^2 [SP1] and 15.2×1.9 μm^2 [SP2], while

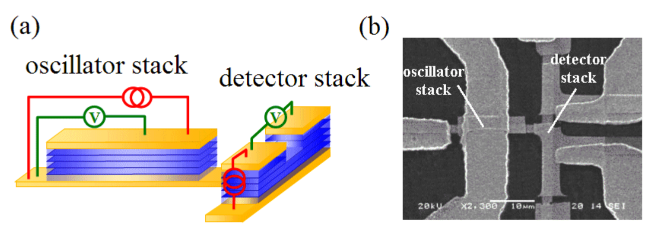

FIG. 1: (color online) (a) Schematic of sample and measurement configurations, showing the oscillator stack (left) and the detector stack (right) of intrinsic Josephson junctions. (b) SEM image of SP2.

the detector stacks were 18×1.3 μm^2 [SP1] and 11.6×2.3 μm^2 [SP2] in their lateral dimensions.

The lower inset of Fig. 2 shows the oscillation of a Josephson vortex-flow resistance (JVFR) of SP1 (N=35) as a function of external magnetic field at T=55 K for a bias current of I_b=2 μA. The field period of the oscillation, 0.51 kG, is one half of H_0 [$=\Phi_0/Ld$=1.02 kG]. Here, H_0 is the magnetic field corresponding to a flux quantum, Φ_0, through each junction of length L (=13.5 μm) and thickness d (=1.5 nm). The $H_0/2$ JVFR oscillation, often observed in the S-shaped embedded structures, is known to originate from the interaction between a triangular vortex lattice and the edge potential for the vortex entry and exit at the junction boundaries [12, 13]. The $H_0/2$ oscillation in our sandwiched oscillator stack thus strongly indicates the formation of the triangular lattice in its low-bias static limit.

The upper inset of Fig. 2 exhibits a single vortex-flow branch corresponding to the near-static triangular lattice in the low-bias region (V<23 mV) and multiple quasiparticle branches in high biases at T=55 K in a transverse field of H=1.2 T; the field denoted by the arrow in the lower inset. In this field range, the single vortex-flow branch persists down to T=4.2 K (not shown). In a higher magnetic field of H=3.9 T as in the region (ii) of the main panel of Fig. 2, however, the single vortex-flow branch splits into multiple vortex-flow sub-branches, which arise as a result of phase-locking of a Josephson vortex lattice on multiple SJP modes [14, 15]. SJP oscillations in each mode, standing along the c axis, propagate along junctions with a characteristic collective mode

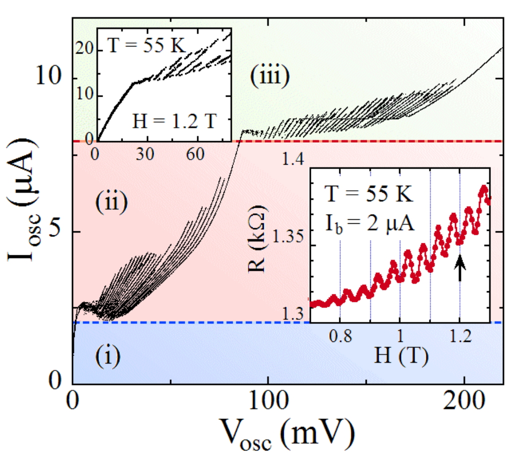

FIG. 2: (color online) I-V characteristics corresponding to the collective Josephson vortex states [(i), (ii), and (iii); refer to the main text] of SP1 for H =3.9 T at T=4.2 K. The contact resistance was numerically subtracted. Upper inset: a single vortex-flow branch (low biases) and quasiparticle branches (high biases) in H=1.2 T at T=55 K, corresponding to the arrow position in the lower inset. Lower inset: Josephson vortex-flow resistance versus external magnetic field of SP1 at T=55 K in a bias current of 2 μA.

velocity [7, 8], $c_n = c_0/\sqrt{1-\cos[\pi n/(N+1)]}$. Here, n (=$1\sim N$) is the mode index and c_0 is the Swihart velocity, which governs the EM-wave propagation in a single Josephson junction.

In SP1 the JVFR oscillations are limited in the current bias range up to $I_b\sim2$ μA. The multiple vortex-flow sub-branches in the bias range of 2 μA< I_b <8 μA are clearly distinguished from the multiple quasiparticle branches above $I_b\sim8$ μA, which corresponds to the critical current for the Josephson pair tunneling in the given magnetic field. In general, a stack of IJJs driven by a bias current in a planar magnetic field is in one of the three different dynamic Josephson-vortex states as illustrated in Figs. 2 and 3(a): (i) the near-static triangular vortex configuration, (ii) the multiple-mode dynamic vortex configuration, and (iii) the irregular vortex configuration corresponding to the McCumber state dominated by the quasiparticle tunneling.

The maximum vortex-lattice velocity is governed by the propagation velocity of a resonating SJP mode in a stack of Josephson junctions. Thus, for the bias beyond $I_b\sim8$ μA, the vortex-flow state transits to the quasiparticle tunneling state as the flowing vortices pass the state of the maximally allowed cut-off voltage, V_{max}, set by the highest plasma velocity in a junction. The maximum vortex-lattice velocity, c_{max}, in SP1 was estimated with V_{max} to be $\sim3.8\times10^5$ m/s using the relation [15] of V_{max}=$NHdc_{max}$. The value of c_{max} in this sandwiched oscillator stack should represent the fastest propagation mode among N collective SJP modes. The Swihart velocity estimated based on the resistively and capacitively shunted junction model [15, 16] turns out to be c_0=2.0×10^4 m/s. Then the corresponding highest in-phase mode velocity, c_1=3.5×10^5 m/s, is in remarkable agreement with the observed value of c_{max} in SP1. This strongly implies that the last sub-branch [the rightmost branch in Region (ii)] corresponds to the in-phase rectangular vortex lattice.

The moving vortex lattice that is in resonance with the collective transverse SJP oscillations is theoretically predicted to emit highly coherent EM waves at a junction edge [8, 17]. The detection of the Shapiro steps, which arise as a result of the resonance between supercurrent oscillations and an irradiated microwave in a Josephson junction [18], would be the most direct confirmation of the electromagnetic emission from the sandwiched oscillator stack, with information on both the frequency and the power of the emission.

Fig. 3(a) shows the bias conditions of the oscillator stack of SP2 (N=28), V_{osc}=38.9, 51.4, 54.4, and 60.8 mV (denoted by filled squares in its vortex-flow branches in the dynamic vortex state) and 100.8 mV (denoted in the quasiparticle branch in the McCumber state), in a field of 4 T at T=4.2 K. In SP2 the detector stack was coupled by the bottom Au electrode with the 2-μm interspacing to the oscillator stack.

The black dI_{det}/dV_{det}-vs-V_{det} curve at the bottom of Fig. 3(b) represents the response of the detector stack

without any bias to the oscillator stack. The curve corresponds to simple nonlinear I-V characteristics without sub-branches in the vortex-flow region (not shown). The pronounced enhancement of the zero-bias conductance is due to Josephson vortex pinning. The vertical dotted lines indicate the positions of V_{max} of the detector stack, where the broad humps are generated by the change in the slope of the detector I-V curves at the boundary between the vortex-flow and quasiparticle tunneling regions. In order to reduce the vortex entry to the detector stack, its width facing the magnetic field (2.3 μm) was designed to be much smaller than that of the oscillator stack. In consequence, not all the IJJs in the detector stack took part in the vortex flow motion. The effective number of vortex-flowing junctions in the detector was estimated to be four by comparing values of V_{max} between the oscillator and detector stacks [19]. Here, we assumed the maximum velocity of the vortices was same in both oscillator and detector stacks [20]. For a selected fixed bias to the oscillator stack in Fig. 3(a), two clear conductance peaks appear in the corresponding dI_{det}/dV_{det}-vs-V_{det} curve of the detector stack: V_{det}^{prim} (V_{det}^{sub})=5.3±0.5 (2.8±0), 6.6±0.2 (3.7±0.2), 7.9±0.3 (4.1±0.2), and 8.5±0.1 (5.2±0.4) mV for four bias conditions in order of increasing voltages in the dynamic vortex state, respectively. Here, V_{det}^{prim} and V_{det}^{sub} are the voltage positions of the primary peak and the subpeak, which are denoted by the upward and the downward arrows, respectively, in Fig. 3(b). The primary conductance peaks are always more evident than the subpeaks. One also notes that the voltage values of peaks in each curve shift in proportion to the increase of the bias voltage V_{osc} of the oscillator stack.

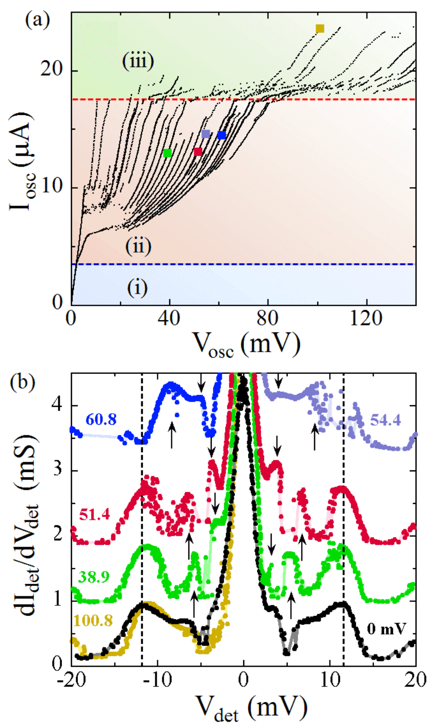

FIG. 3: (color online) (a) Collective Josephson-vortex-flow multiple sub-branches and bias voltages V_{osc} (filled squares) of the oscillator stack of SP2 for H=4 T at T=4.2 K. The contact resistance was numerically subtracted. The two horizontal dashed lines divide the I-V characteristics into three regions as in Fig. 2. (b) Responses of the detector stack revealed in its differential conductance corresponding to the biases of the oscillator in (a). Each curve is shifted vertically for clarity.

To confirm that the observed peaks are indeed the response of the detector stack to the irradiation [21], the voltages of the conductance peaks (v_{det}) are plotted in Fig. 4(a) as a function of the bias voltage v_{osc}. Here, v_{osc} ($\equiv V_{osc}/N_{osc}$) and v_{det} ($\equiv V_{det}/N_{det}$) are normalized by the number of junctions involved in the vortex flow in the oscillator and the detector stacks (N_{osc}=28 and N_{det}=4), respectively. For the primary peaks, the values of v_{osc} are in excellent accordance with the values of v_{det}, which confirms that the primary peaks were caused by the Josephson ac response, *i.e.*, integer Shapiro steps [22]. Frequencies corresponding to V_{osc}=38.9, 51.4, 54.4, and 60.8 mV are 0.67, 0.87, 0.94, and 1.06 THz, respectively [23]. For the bias conditions of V_{osc}=54.4 and 60.8 mV, the humps at V_{max} in Fig. 3(b) smear out, as the outward-shifting positions of the conductance peaks overlap with those of V_{max}.

On the other hand, in Fig.3(b), the voltage positions of the conductance sub-peaks turn out to be one half of V_{det}^{prim}. The relation between the two kinds of peaks in terms of reduced parameters is shown in Fig. 4(a). These half-integer Shapiro steps are believed to be caused by phase locking of the second harmonics of the Josephson oscillations on the primary frequencies [24]. For the bias voltage of 100.8 mV in the quasiparticle tunneling state of the oscillator stack, without the vortex-lattice formation along the c axis, no effective vortex-flow-induced emission is expected. Thus, as in Fig. 3(b), the response of the detector without any Shapiro-step peaks in this bias is almost identical to the zero-bias curve represented by the black curve.

The irradiation power, P, is estimated from the approximate relation [25], $P{\sim}\Delta I_1^2 V_1 \Omega^2 \beta_c/2I_c$, where ΔI_1 is the height of the Shapiro current step, V_1 is the voltage value of the primary peak position in N-stacked junctions, $\Omega^2\beta_c{=}(\pi h/e)(\epsilon f^2/tJ_c)$, $\Omega{=}f/f_c$ is the irradiated-wave frequency normalized by the characteristic frequency $f_c{=}2eI_cR_n/h$, β_c is the McCumber parameter, ϵ is the dielectric constant, t(=1.2 nm) is the spacing between neighboring CuO_2 layers, and I_c (J_c) is the tunneling critical current (density). The value of ΔI_1 is estimated using the relation $\Delta I_1{=}\Delta V_1 \frac{dI}{dV}|_{prim}$, where ΔV_1 is the voltage width of the primary peak [22] estimated at the base level of each curve in Fig. 3(b). Fig. 4(b) illustrates that the estimated power irradiated onto the detector stack increases rapidly for lower-index modes; P=0.69±0.14, 1.01±0.16, 7.5±0.7, and 15.9±0.5 nW for the biases of v_{osc}=1.39, 1.84, 1.94, and 2.17 meV, respec-

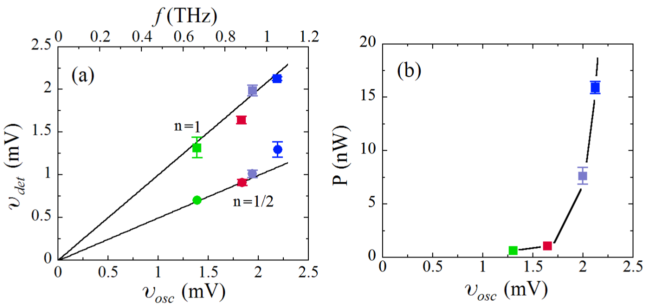

FIG. 4: (color online) (a) Primary (n=1) and sub-harmonic (n=1/2) conductance-peak voltages in the detector stack, corresponding to the integer and the half-integer Shapiro steps, respectively, with the emission frequencies denoted in the upper horizontal axis. (b) Estimated power irradiated on the detector stack for each bias condition in the oscillator stack.

tively. The emission power from the SJP modes is indeed theoretically predicted to grow for lower-index modes as the emitted waves become more phase-coherent and reaches a maximum for the completely in-phase mode corresponding to n=1 [8]. One also notices that the two bias conditions V_{osc}=51.4 and 54.4 mV in Fig. 3(a), although in the same branch, result in a large difference in the estimated irradiation power as in Fig. 4(b). This takes place because, as the vortex motion approaches the resonance condition in a branch, the energy fed by the bias is consumed more for an emission rather than speeding up the vortex lattice. This observed emission from the vortex-flow region well justifies the excitation picture of the SJP modes themselves. A more effective impedance matching scheme between the oscillator and the detector stacks by combining proper antennas in the system is expected to generate clearer Shapiro steps with higher emission power.

In the presence of Josephson vortices a Josephson junction itself is bound to exhibit a distributed Shapiro-step response even to the monochromatic irradiation [22]. Thus, the finite Shapiro-step peak width in Fig. 3(b) does not necessarily represent the frequency distribution in the emitted waves, which can be determined by the heterodyne detection instead [21, 27].

The vortex-flow terahertz generation in stacked Bi-2212 IJJs has the great advantage of continuous and frequency-tunable nature of the generated waves. The coherency of the terahertz emission from the rectangular vortex-lattice configuration is another advantage of vortex-flow technique over, for instance, the radiation in a quasiparticle-tunneling region where the phase coherence is lacking between radiations from adjacent junctions. The direct detection of emission in this study provides an additional noble scheme of developing solid-state terahertz emission sources [28] that eventually helps bridge the terahertz gap.

This work was supported by the National Research Laboratory program administrated by Korea Science and Engineering Foundation (KOSEF). This paper was also supported by POSTECH Core Research Program.

[1] B. Ferguson and X.C. Zhang, Nat. Mater. **1**, 26 (2002).
[2] R. Köhler *et al.*, Nature **417**, 156 (2002).
[3] G. L. Carr *et al.*, Nature **420**, 153 (2002).
[4] K. Kawase *et al.*, Appl. Phys. Lett. **80**, 195 (2002); W. Shi and Y. J. Ding, Appl. Phys. Lett. **84**, 1635 (2004).
[5] E. J. Singley *et al.*, Phys. Rev. B **69**, 092512 (2004).
[6] R. Kleiner *et al.*, Phys. Rev. Lett. **68**, 2394 (1992).
[7] S. Sakai, P. Bodin, and N. F. Pederson, J. Appl. Phys **73**, 2411 (1993); R. Kleiner, Phys. Rev. B. **50**, 6919 (1994).
[8] M. Machida and M. Tachiki, Curr. Appl. Phys. **1**, 341 (2001).
[9] V. P. Koshelets and S. V. Shitove, Supercond. Sci. Technol. **13**, R53 (2000); G. Hechtfischer *et al.*, Phys. Rev. Lett. **79**, 1365 (1997); M.-H. Bae and H.-J. Lee, Appl. Phys. Lett. **88**, 142501 (2006); M.-H. Bae and H.-J. Lee, IEICE Trans. electron., **E89-C**, 106 (2006).
[10] H. B. Wang, P. H. Wu, and T. Yamashita, Appl. Phys. Lett. **78**, 4010 (2001).
[11] M.-H. Bae *et al.*, Appl. Phys. Lett. **83**, 2187 (2003).
[12] S. Ooi, T. Mochiku, and K. Hirata, Phys. Rev. Lett. **89**, 247002 (2002); S. M. Kim, *et al.*, Phys. Rev. B **72**, 140504(R) (2005).
[13] M. Machida, Phys. Rev. Lett. **90**, 037001 (2002); A. E. Koshelev, Phys. Rev. B **66**, 224514 (2002); Recently, M. Machida proposed [Phys. Rev. Lett. **96**, 097002 (2006)] that the edge potential effect also form a rectangular lattice in a steady state for a sufficiently short stack of junctions.
[14] J. U. Lee *et al.*, Appl. Phys. Lett, **71**, 1412 (1997).
[15] M.-H. Bae and H.-J.Lee, Phys. Rev. B **70**, 052506 (2004).
[16] A. Irie, Y. Hirai, and G. Oya, Appl. Phys. Lett, **72**, 2159 (1998).
[17] M. Tachiki *et al.*, Phys. Rev. B **71**, 134515 (2005).
[18] Y.-J. Doh *et al.*, Phys. Rev. B. **61**, R3834 (2000); H. B. Wang, P. H. Wu, and T. Yamashita, Phys. Rev. Lett. **87**, 107002 (2001).
[19] H. B. Wang *et al.*, Appl. Phys. Lett. **88**, 063503 (2006).
[20] G. Carapella and G. Costabile, Appl. Phys. Lett. **71**, 3412 (1997); G. Hechtfischer *et al.*, Phys. Rev. B **55**, 14638 (1997).
[21] A. V. Ustinov *et al.*, IEEE Trans. Appl. Supercond. **7**, 3601 (1997).
[22] Yu. I. Latyshev *et al.*, Phys. Rev. Lett. **87**, 247007 (2001).
[23] The frequency is estimated based on the frequency-voltage (per junction) conversion relation, f=2eV_{osc}/Nh (=483.6 GHz/mV$\times V_{osc}/N$).
[24] K. K. Likharev, *Dynamics of Josephson Junctions and Circuits* (Gordon and Breach, New York, 1986).
[25] For the power formula, we used P=$I_{ac}^2 R_{in}/2$, where I_{ac} is the ac current amplitude of irradiated waves, $R_{in}(=N/2\pi fC)$ is the input impedance and C is the capacitance of a junction [26]. Since the irradiated power is

expected to be low enough in this study the height of the current step varies in linear proportion to the irradiated power, resulting in $\Delta I_1 \approx I_{ac}/\beta_c\Omega^2$.

[26] S. Rother, Ph.D. Thesis. (Physikalisches Institut III, Universität Erlangen-Nürnberg, Germany, 1998).

[27] I. E. Batov *et al.*, Appl. Phys. Lett. **88**, 262504 (2006).

[28] K. Kadowaki, Sci. and Technol. Adv. Mater. **6**, 589 (2005); S. Savel'ev *et al.*, Nature Physics **2**, 521 (2006).